3 – DIMENSIONAL COMPUTATIONAL ANALYSIS OF FLUID FLOW AROUND MICRO FLOW SENSOR AT DIFFERENT POSITIONS AND PILLAR ARRANGEMENTS

TONY TAN HIN JOO

UNIVERSITI SAINS MALAYSIA
2008

ACKNOWLEDGEMENT

I would like to take this opportunity to express my special thanks to my supervisor, Dr. Mohd. Zulkifly Bin Abdullah, who gave me a lot of advice and guidance in conducting the research.

Again, I also want to thank my supervisor as well as USM for giving financial support to me during my study.

Besides this, special thanks are also given to Dr. Al – Badlishah, Mr. Roslan (Technician) and Mr. Amir (Technician) from Electrical And Electronic Engineering School, who gave me technical supports for completion of the research.

Lastly, I would like to thank my parents who gave me continuous supports during the whole research.

CONTENTS

LIST OF TABLES

LIST OF FIGURES

LIST OF ABBREVIATIONS

CFD	**Computational Fluid Dynamic**
FVM	**Finite Volume Method**
FDM	**Finite Difference Method**
Exp.	**Experimental**
MAC	**Marker and Cell Method**

NOMENCLATURES

u, v, w	**velocity in directions of x, y, and z, m/s**
T	**temperature, K**
Re	**Reynolds number**
ρ	**density, kg/m^3**
μ	**dynamic viscosity of fluid, Ns/m^2**
p	**pressure, Pa**
t	**time, s**
c_p	**specific heat of fluid flow, J/kg K**
k	**conductivity of fluid flow, W/m K**
U_{max}	**velocity maximum, m/s**
ν	**kinematic viscosity, m^2/s**
∇	**vector differential operator, $(\frac{\partial}{\partial x}+\frac{\partial}{\partial y}+\frac{\partial}{\partial z})$**
x, y, z	**variable in physical plane**
ξ, η, ϕ	**variable in computational plane**

LIST OF REFERENCES

ANALISA KOMPUTERAN TIGA DIMENSI BAGI ALIRAN BENDALIR DI SEKITAR PENDERIA ALIRAN MIKRO PADA PERBEZAAN POSISI DAN SUSUNAN TIANG

ABSTRAK

Analisis pengaliran bendalir mengelilingi pengesan mikro telah dipamerkan dalam penyelidikan ini. Dalam analisis tersebut, pengesan mikro dianggap dipasangkan dalam saluran berbentuk segi empat tepat. Dua langkah penting telah diambil iaitu mengoptimumkan rekebentuk pengesan mikro dan kecekapan pengesanannya. Kaedah Perbezaan Terhingga telah dipilih sebagai penyelesaian utama bagi menyelesaikan persamaan-persamaan seperti Persamaan Keselanjaran, Persamaan 'Navier-Stokes', dan Persamaan Tenaga. Dengan itu, penyelesaian daripada persamaan-persamaan tersebut boleh digunakan dalam proses visual untuk memerhatikan kontur pengaliran bendalir mengelilingi pengesan mikro. Kaedah 'MAC' yang dikenali sebagai 'Marker And Cell' juga telah diaplikasikan dalam analisis tersebut bagi menyelesaikan bahagian tekanan dalam persamaan 'Navier-Stokes'. Bagi membolehkan proses pengiraan yang kompleks berjalan dengan efektif, semua penyelesaian persamaan-persamaan diprogramkan ke dalam FORTRAN 77. Kemudian, hasil keputusan dari pengiraan tersebut disimpan dalam fail keputusan, di mana keputusan tersebut akan digunakan untuk menghasilkan kontur pengaliran bendalir mengelilingi pengesan mikro dalam bentuk visual. Proses mengoptimumkan kecekapan pengesanan mikro pengesan yang dijalankan adalah berdasarkan kepada ketebalan lapisan sempadan yang disimulasikan pada permukaan atas mikro pengesan. Kesan nombor Reynolds, ketinggian pengesan mikro dari permukaan saluran, bilangan / susunan penyokong, ruang udara dalam mikro pengesan dan orientasi juga diambilkira dan mendapati bahawa peningkatan nombor tersebut boleh

meningkatkan kesan pengesanan pengesan mikro. Selepas menjalankan analisis dengan terperinci, didapati bahawa ketebalan bagi kedua-dua lapisan sempadan hidro-dinamik dan terma kurang dengan peningkatan nombor Reynolds. Dengan adanya ruang udara dalam strukturnya, kadar kehilangan tenaga melalui struktur pengesan tersebut dapat dikurangkan dengan berkesan. Oleh yang demikian, pengesan mikro yang optimum mesti mempunyai ciri-ciri seperti: disokong dengan empat unit penyokong, berorientasi secara tangen, disokong pada ketinggian 0.5mm dari permukaan dinding saluran, dan mempunyai ruang udara dalam strukturnya.

3 – DIMENSIONAL COMPUTATIONAL ANALYSIS OF FLUID FLOW AROUND MICRO FLOW SENSOR AT DIFFERENT POSITIONS AND PILLAR ARRANGEMENTS

ABSTRACT

The numerical analysis of fluid flow around micro flow sensor is presented in the research. The sensor is assumed as installed in a rectangular channel. There are two approaches that have been performed in order to optimize the sensor design and obtain optimum sensing efficiency of the sensor. The finite difference method has been chosen as the primary solution procedure for the Continuity equation, Navier – Stokes equation and Energy equation in order to predict the non – linear rotational physics of fluid flow around the sensor. MAC method, which is known as 'Marker And Cell', is applied to solve for the pressure term in Navier – Stokes equation. To ensure effective calculation process, all solutions of governing equations are coded into FORTRAN 77. Then, the results of the calculation will be stored into result file and visualized in order to observe the fluid flow contour around the sensor. The optimization of micro flow sensor is conducted based on the boundary layers thickness that developed on the top surface of the sensor. The effect of Reynolds Number, air cavity inside sensor body, height of sensor above surface channel, and number / arrangement of pillar are investigated and it was found that these effects are significant on the boundary layer thickness that is produced on the top surface of the sensor. After detail investigation, the increase of Reynolds number shows obvious improvement on the sensor sensing efficiency at tangential position, with four pillars arrangement and at the pillar height of 0.5mm above the channel wall surface. In addition, by introducing air cavity into micro flow sensor body, the energy loss through sensor can be reduced effectively.

CHAPTER 1

INTRODUCTION

1.1 General

After the development of micro technology which is known as Micro Electro Mechanical Systems (MEMS), the design of flow sensor in micro size becomes more important. The purpose of the design is to overcome the difficulties that arose in flow measurement, especially in a very small space in which conventional sensor can not perform measurement as required. Even there are many kinds of micro flow sensor that had been designed or produced recently, some of them still cannot meet the requirement in certain flow measurement condition. There are several factors that affected them, such as size, shape, type of function, etc.

In order to overcome the problems mentioned above, the optimization analysis on micro flow sensor design has been performed and presented in this study. The finite difference method has been applied in order to solve the governing equations, which are continuity equation, Navier–Stokes Equations, and Energy equation. By solving these equations, the fluid flow around the micro flow sensor can be described and simulated as proposed by Kawamura and Kuwahara (1984 and 1985). The MAC method has also been applied to solve the pressure term in Navier–Stokes equations. The numerical formulation has been programmed using Fortran77 programming language. Then, the solutions are visualized into graphical forms in which the fluid flow around micro flow sensor can be observed clearly.

There are two positions of micro flow sensor that are taken into consideration, i.e. diagonal position and horizontal position. For each position, different types of sensor designs (**non pillar** sensor, **single pillar** sensor, **two pillars** sensor, and **four pillars**

sensor) are also taken into consideration. In this study, three stages of optimization analysis are performed, i.e. determination of optimum height of sensor, analysis of air cavity effect inside sensor body, and analysis of optimum pillar arrangement of sensor.

The main function of the micro flow sensor, which is presented in this research work, is using the heat dissipation to measure the velocity and temperature of the fluid flow. It is designed and installed in a micro channel with height of 3.0mm. Sample of the micro flow sensor can be seen from Figures 1.1 and 1.2.

Figure 1.1: Micro Flow Sensor At Diagonal Position In Conduit

Figure 1.2: Cross Sectional View of Conduit Containing Micro Flow Sensor

1.2 Objectives

The main purpose of the research is to design an effective micro flow sensor that would help to meet the requirement of engineering technology, especially in the engineering parameters measurement. The new micro sensor is to replace the role that was played by conventional sensor. This is because of some circumstances which will not allow the conventional sensor to do measurement since the available space is too small. For example in the micro channel and small pipeline in which their cross – sectional area are very small. Besides this, even the more sophisticated micro sensors have been designed and available in the market but in some conditions, the conventional sensor still cannot meet the specific engineering measurement, which is restricted by several factors such as shape and type of function. In order to overcome the difficulties, the following factors have been identified and analyzed, and presented as well in the present research work:

a. To study the effect of sensor position in fluid flow.

b. Height of sensor above channel surface.

c. Pillars arrangements beneath sensor body.

d. Effects of different Reynolds number on the sensor performance.

e. Effect of air cavity inside sensor body.

All the factors above are analyzed based on the hydrodynamic boundary layer thickness and thermal boundary layer thickness at the top surface of micro flow sensor. Hydrodynamic and thermal boundary layers thicknesses are chosen as primary parameters in determining the sensing efficiency of micro flow sensor, because the thinner boundary layers can produce low drag and high heat transfer coefficient. As a result, the heat transfer through boundary layers thickness is high and the sensing efficiency of the micro flow sensor will increase.

1.3 Problem Statements

There are several problems associated with conventional sensors:

a. The size of conventional sensor is large and it can not be installed in a very small space.

b. The conventional sensor design, that uses heat dissipation for measurement, does not have energy saving concept. As a result, the heat that is generated from sensing element loss through its structural body.

c. The sensitivity of conventional sensor needs improvement in terms of drag and heat transfer performance. These can be improved by considering the orientation position, the height of sensor, and the sensor structural design.

1.4 Principle of Thermal Mass Flow Meters For Conventional Flow Sensor

Flow of fluid can be seen as the motion of continuum in a closed structure and is the object of measurement. The related physical quantity that are taken into account in engineering measurement is the mass flux which flows through a unit cross-section. Thermal mass flow measurement is a basic principle for most common conventional flow sensor. They convert the mechanical variable (mass flow) via thermal variable (heat transfer) into electrical signal, in which the signal can be processed to indicate essential result of the flow.

Figure 1.3 shows the basic function of conventional flow sensor as follow:

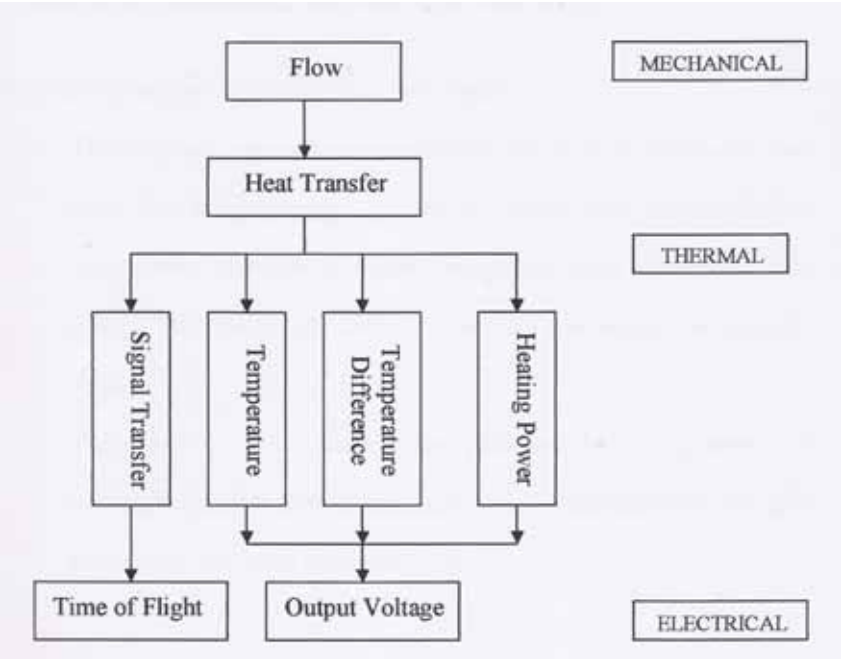

Figure 1.3 The basic function of conventional flow sensor

1.5 Literature Reviews

In the study of optimum design of micro thermal flow sensor that was conducted by Yoshino et al. (2003), two types of analysis have been performed i.e. numerical analysis and experimental investigation. In their research work, the design of micro thermal flow sensor is as shown in the Figure 1.4:

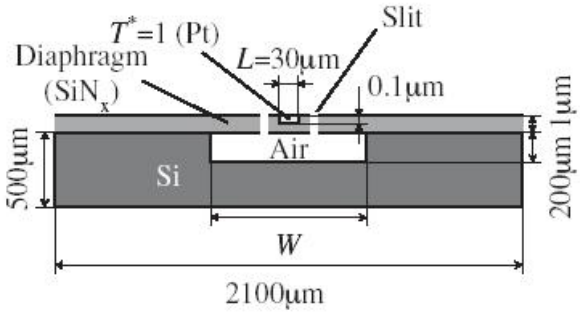

Figure 1.4: Schematic of sensor model (not to scale) (Yoshino et al. 2003).

The purpose of the research work was to perform an analysis of unsteady conjugate heat transfer for micro thermal flow sensor in order to improve its frequency response in the wall shear stress measurement. The fluid flow over the sensor was assumed as air and in turbulent flow condition. The sensor contains air inside its body, which act as heat resistance, in order to reduce heat loss through its body. In the numerical analysis, they apply two–dimensional computational model to predict the temperature distribution above the sensor surface in the air flow stream. Figure 1.5 shows the two–dimensional computational model that was used in the study.

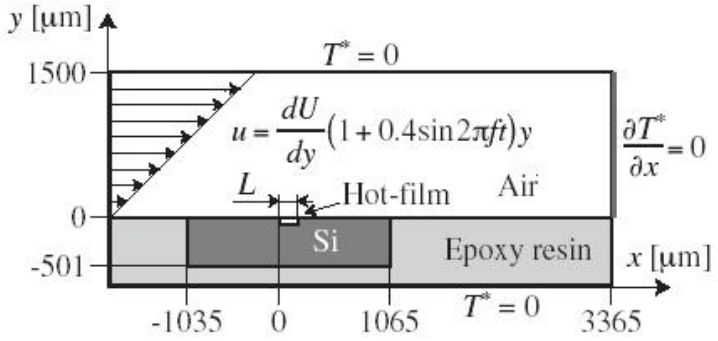

Figure 1.5: Computational domain and boundary condition (Yoshino et al. 2003).

In order to mimic the fluctuating flow velocity near the wall, the fluid velocity was given as a linear function of the distance to the wall. Since the velocity profile is given, the following governing equation was used for thermal field, i.e.: $\frac{\partial T^*}{\partial t^+} + u^+ \frac{\partial T^*}{\partial x^+} = \frac{1}{\mathrm{Pr}}(\frac{\partial^2 T^*}{\partial x^{+^2}} + \frac{\partial^2 T^*}{\partial y^{+^2}})$; where x^+ and y^+ denote non–dimensionalized distance using the mean velocity gradient at the wall $\frac{dU}{dy}$ and the kinematic viscosity, ν. The response of the sensor models having thermal insulation slit on the both sides of the hot–film are examined numerically. As shown in Figure 1.6(a), the extent of 'thermal cloud' is confined between the slits, and contour of the temperature field becomes dense especially close to the slits. Figure 1.6(b) shows temperature distribution of the sensor model assuming a vacuum cavity underneath the diaphragm. The temperature distribution spreads out to the upstream and downstream directions due to the heat conduction in fluid, and this 'thermal cloud' inhibits the hot–film to be exposed to the ambient temperature. Therefore, sensors with air cavity and slits on the diaphragm should have superior response than the sensor with continuous diaphragm and vacuum cavity underneath.

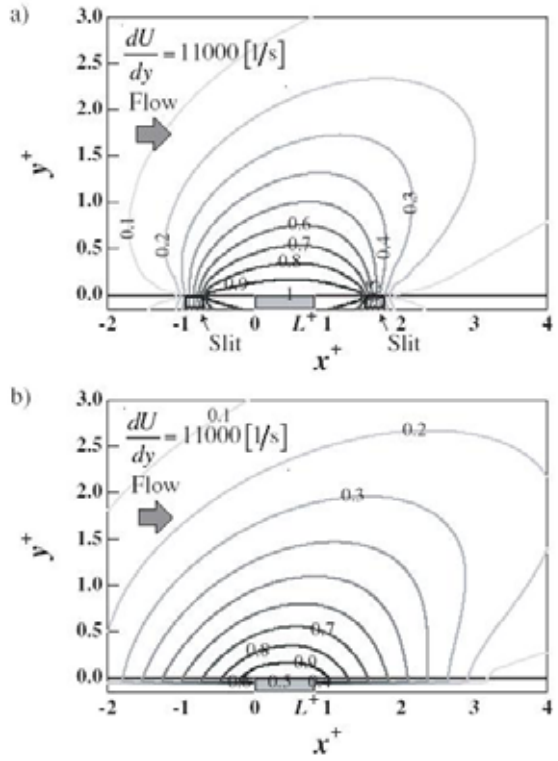

Figure 1.6: Temperature distribution around the sensor model. a) With slit and air cavity, b) Without slits and vacuum cavity (Yoshino et al. 2003).

In the experimental approach, two types of sensor models have been fabricated and analyzed, as indicated in Figures 1.7 and 1.8. The experiment was conducted in the turbulent channel flow facility having a channel width of 50mm. The bulk mean velocity is 2.5 – 9.3m/s.

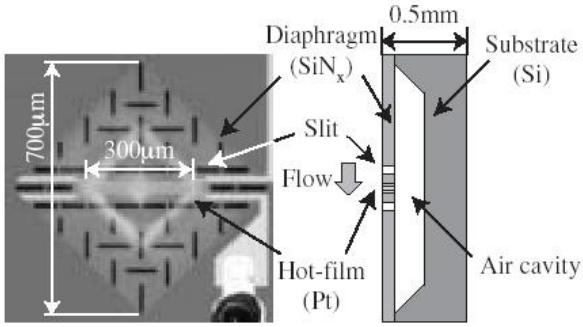

Type 1

Figure 1.7: Magnified view of micro hot – film shear stress sensor (Yoshino et al. 2003).

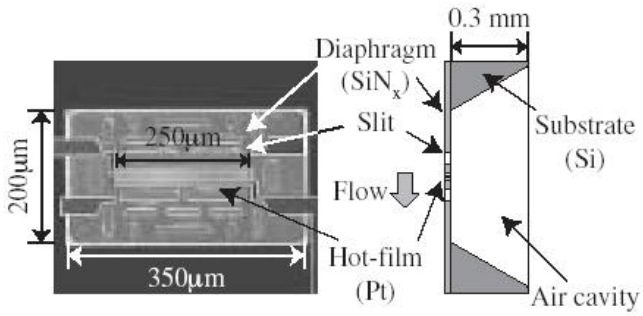

Type 2

Figure 1.8: Magnified view of micro hot – film shear stress sensor (cont') (Yoshino et al. 2003).

The frequency response of Type 2 was found to be significantly better than that of Type 1. This is because of the diaphragm length effect in both of the sensor models, i.e. between 200μm and 700μm in diaphragm width. Hence, the shorter diaphragm length produces better performance in response. Finally, they concluded that heat conduction to the fluid has large effect on the sensor response and the sensor which have deep air cavity exhibit better performance than vacuum cavity sensor.

Wu et al. (2001) has studied the effect of suspended microchannel from substrate in order to determine the improvement of thermal isolation as shown in Figures 1.9 and 1.10. His study was conducted in two ways, i.e. numerical analysis and experimental analysis.

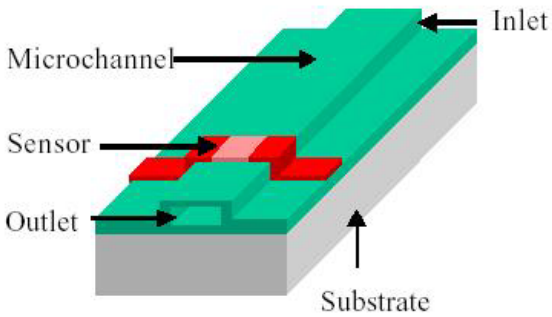

Figure 1.9: A microchannel – based flow sensing approach (Wu et al. 2001).

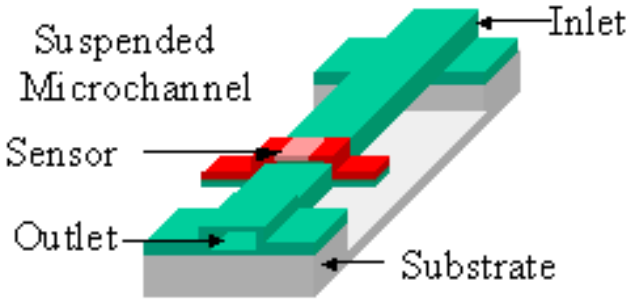

Figure 1.10: An improved flow sensing approach with a suspended microchannel (Wu et al. 2001)

Figure 1.11 shows the three designs of microchannel flow sensors that have been analyzed in the research work.

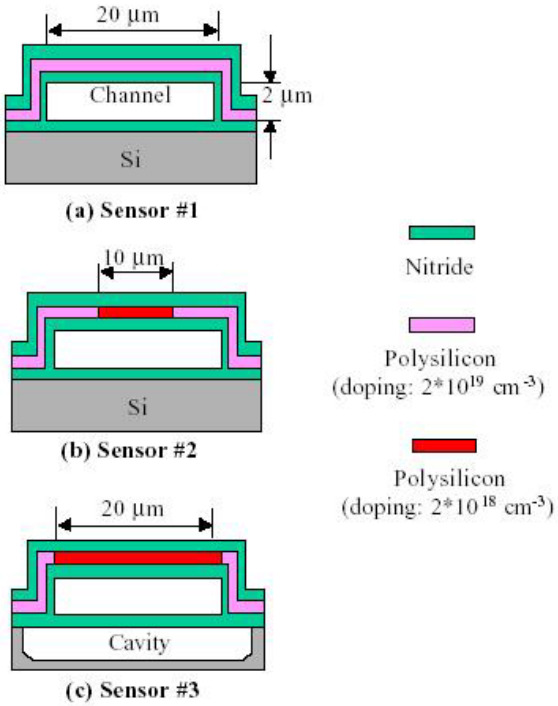

Figure 1.11: Three flow sensor designs (Wu et al. 2001).

They found that the suspended flow sensor gives the best result of temperature – to – flow ratio (0.026 °C/nL/min) approximately 5 times better than the first two sensors. The results have been compiled into the Figure 1.12.

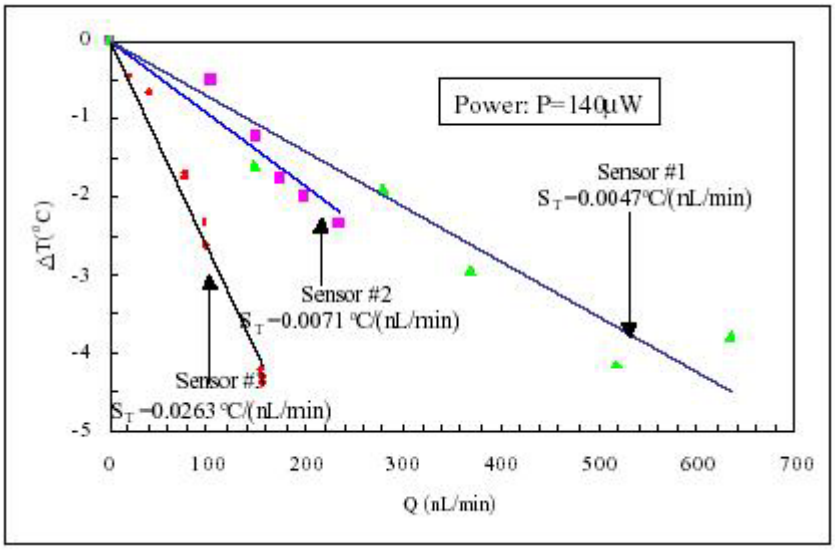

Figure 1.12: Temperature change of the sensors due to liquid flow (Wu et al. 2001).

This phenomenon shows that better thermal isolation can be achieved by channel suspension in order to obtain better sensitivity. The flow – induced sensor temperature changes as a function of flow rate is plotted in the Figure 1.13 for sensor no.3 along with the experimental data.

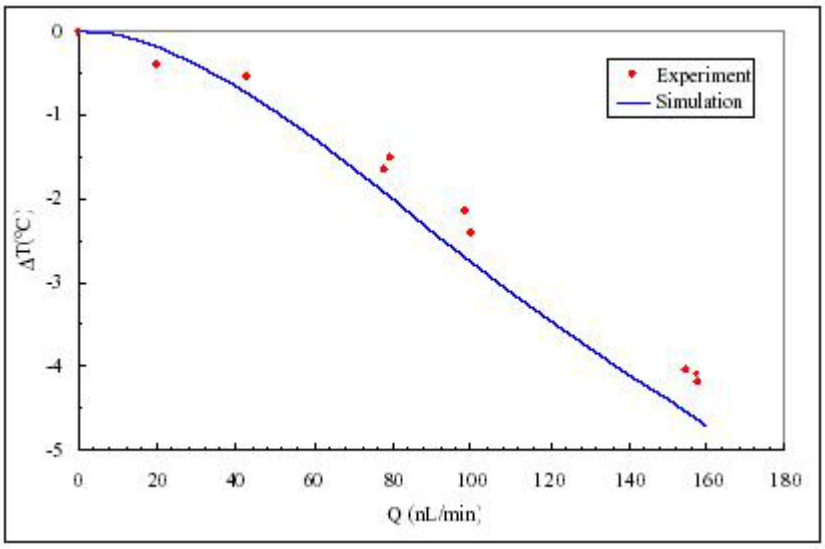

Figure 1.13: Simulated vs. measured flow – induced temperature change for sensor no.3 (Wu et al. 2001).

There is a good agreement between theory and experiment. In figure 1.13, $\Delta T(°C) = T(Q) - T(0)$; where T(Q) is the heater temperature as a function of flow rate and T(0) is the initial heater temperature. As the liquid flow increases, the flow – induced temperature in the micro channel reduces. Finally, the sensor design not only can measure the flow rates, but also detect the presence of air bubbles. Since air has a lower heat capacity and conductivity than water, the sensor can detect a sudden temperature rise, as shown in Figure 1.14.

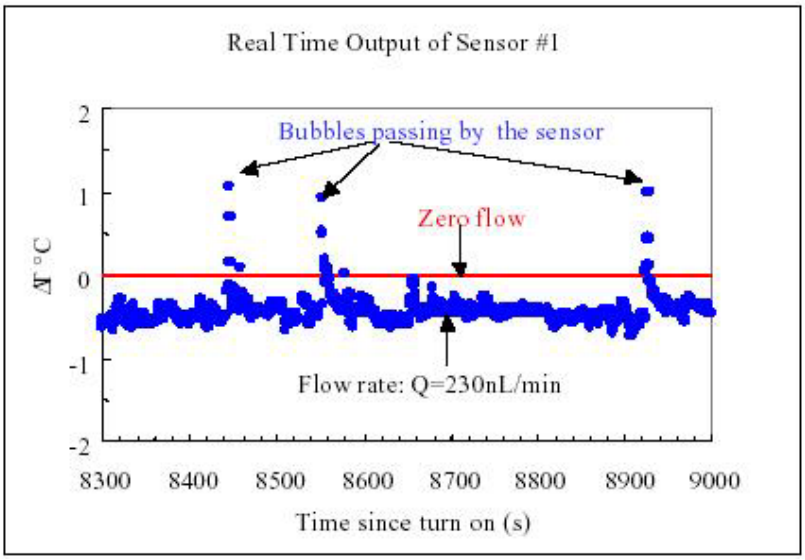

Figure 1.14: Real time output of sensor #1. Temperature spikes indicate passage of an air bubble (Wu et al. 2001).

Thus, they concluded that removing a portion of silicon substrate underneath the sensor better gave thermal isolation.

Wu et al. also studied a suspended micro channel with integrated temperature sensors for high – pressure flow studies. These microchannels are approximately 20µm x 2µm x 4400µm, and are suspended above 80µm deep cavities. Experimental study of gas and liquid flow through the microchannel under high inlet pressures was conducted. Theoretical analysis was also conducted with an analytical model developed for capillary flow that accounts for 2D, slip and compressibility and corrected for flow acceleration and non – parabolicity. The resulting change in channel geometry has also been considered under high pressures. Figure 1.15 shows the cut – section of suspended microchannel integrated with temperature sensor.

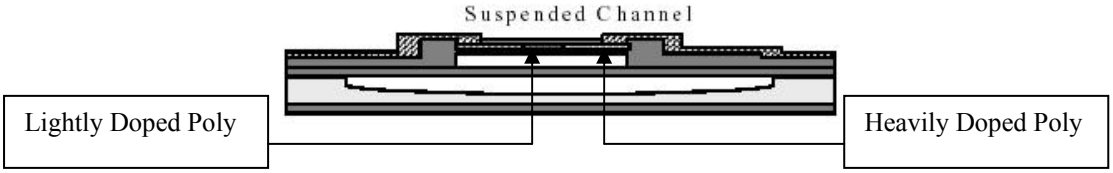

Figure 1.15: Schematic of suspended microchannel integrated with temperature sensor (Wu et al.).

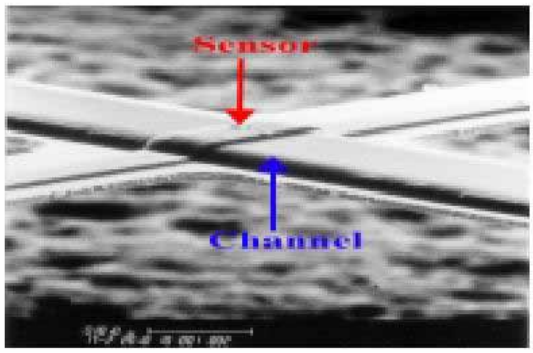

Figure 1.16: SEM of a freestanding channel with a temperature sensor embedded onto the top wall (Wu et al.).

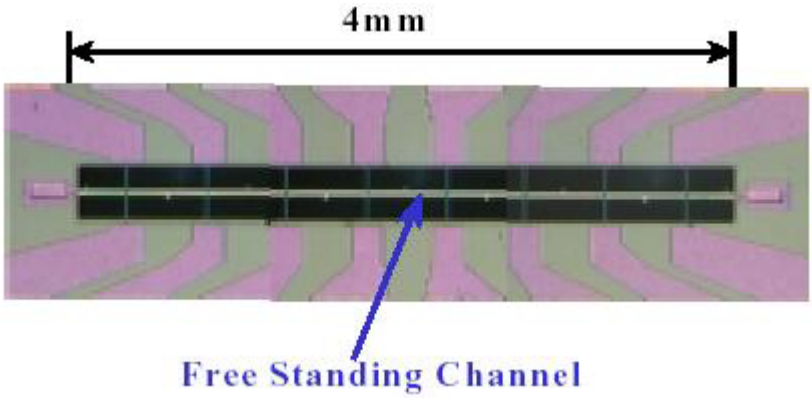

Figure 1.17: Photograph of the top view of a free standing microchannel (Wu et al.).

Berberig et al. (1998) has designed a micro flow sensor known as Prandtl Micro Flow Sensor, which is a novel silicon diaphragm capacitive sensor for flow – velocity measurement. Figure 1.18 below that shows the detail of sensor structure.

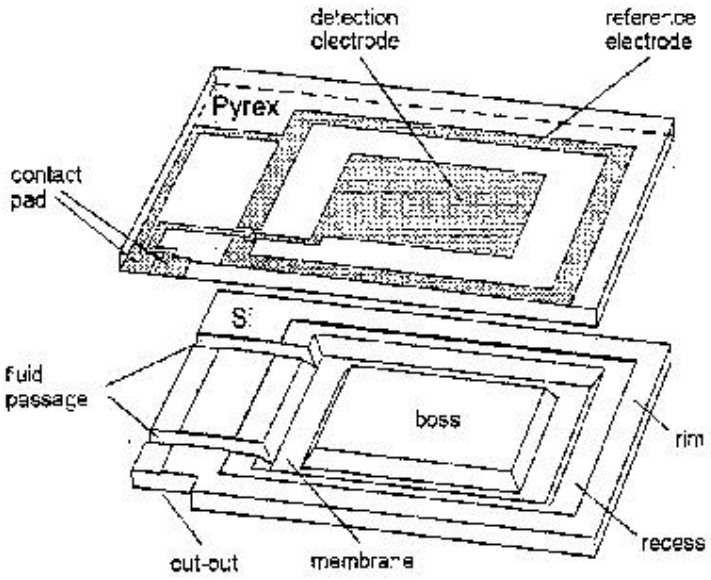

Figure 1.18: Exploded view of the sensor structure (Berberig et al. 1998).

The sensor consists of two plates and both plates enclose a cavity that forms a detection and reference capacitor between the electrodes on the glass, and the boss and the recess, respectively. The flowing fluid will flow through the fluid passage and filled into the cavity of the sensor. Then, the fluid velocity is measured by simple electrical connection of the detection electrode. The main purpose of the fluid passage is the transmission of the stagnation pressure into the sensor cavity. Theoretically, the simulation of flow around the micro flow sensor is based on the Bernoulli equation, $\rho gz + p_{stat} + \frac{\rho v^2}{2} = const.$, where ρ = fluid density, g = gravity, z = height, p = pressure, and v = velocity. Although the Bernoulli equation is only valid for inviscid and incompressible fluid flow, the application of the equation is limited to the

measurement of velocities up to about 100 ms^{-1}. Fluid flow with velocity below 100 ms^{-1} can be taken as incompressible, in which the gas density can safely be assumed to be constant. Figure 1.19 shows the operation principal of the sensor.

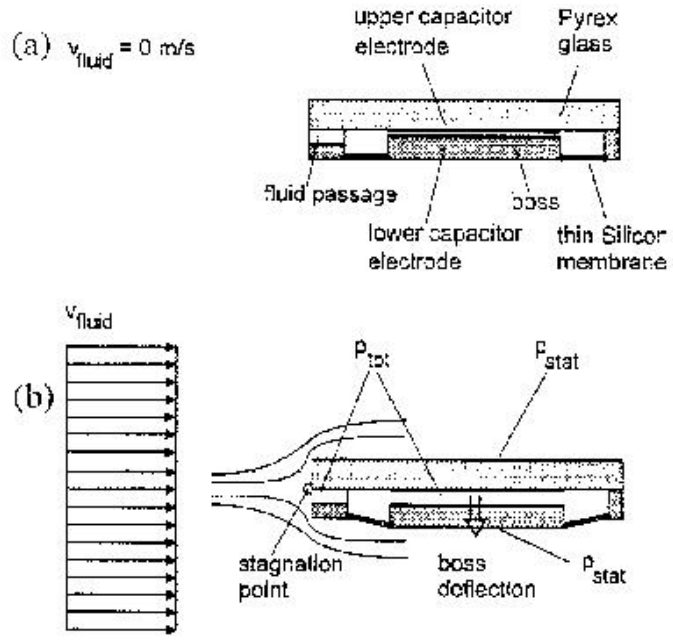

Figure 1.19: Operation principle of the sensor (Berberig et al. 1998).

When the fluid flows through the fluid passage into and fills the cavity of the sensor, the diaphragm with a solid weight at its center is deflected. The deflection is directly proportional to the external force and produces small displacements. At the same time, the small displacements also occurred at capacitor electrodes and yield an approximately linear relation between electrode gap height and capacitance. This capacitance change is converted into a voltage by an appropriate circuit, and then related to the fluid flow velocity. The fabrication of the sensor and experimental measurement on the sensor were also carried out inside a small wind tunnel that can generate air velocity of up to 25ms^{-1}. The comparison between the experimental results and analytical results indicated that the sensor sensitivity was low. This is

because of the unfavorable ratio of Si wafer thickness (t_{Si}=0.2mm) to Pyrex plate thickness (t_{Py}=1.2mm) which is causing significant reduction of the pressure inside the PMFS (Prandtl Micro Flow Sensor) cavity. Figure 1.20 shows the comparison results between experimental and analytical approach.

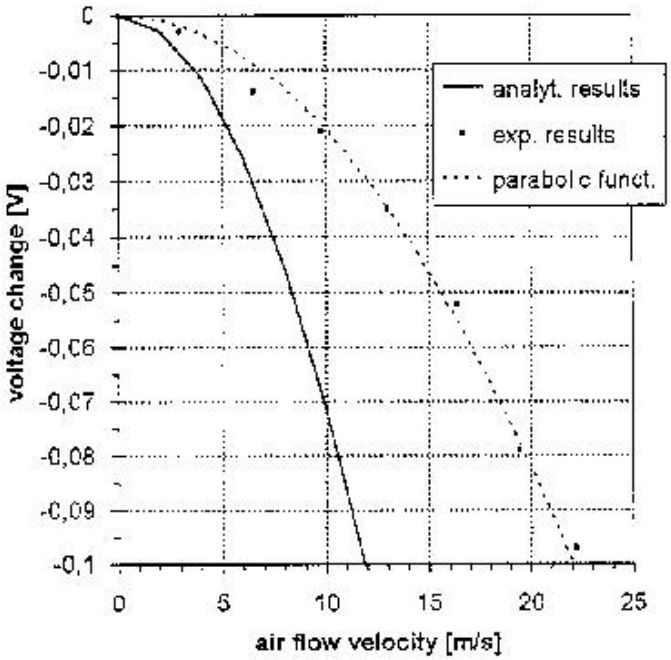

Figure 1.20: Readout signal as a function of flow velocity (Berberig et al. 1998).

In the electrochemical time of flight flow (TOF) sensor, the detection of oxygen in the micro sensor is applied. This sensor design is made by Wu and Sansen (2002). Figure 1.21 shows the cross section of the micro TOF flow sensor.

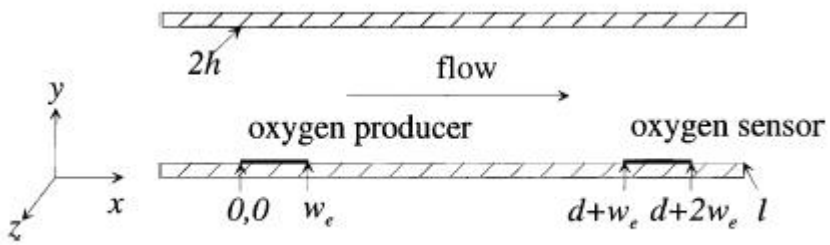

Figure 1.21: The cross section of the micro TOF flow sensor (both oxygen producer and oxygen sensor consist of a working electrode respectively. Only the working electrodes of both cells are shown for simplicity) (Wu and Sansen, 2002).

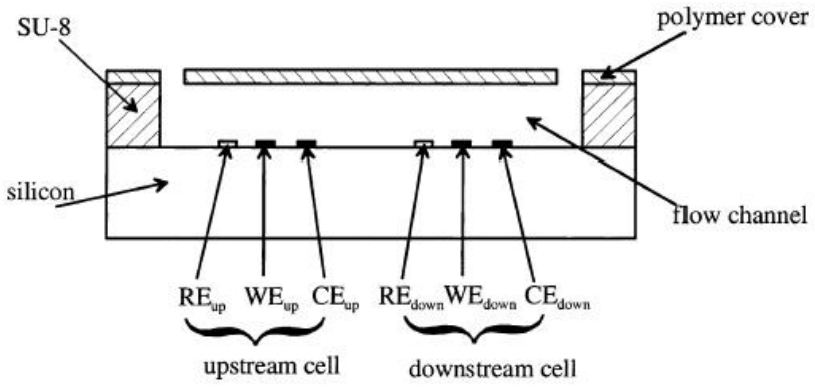

Figure 1.22: The cross section of the fabricated TOF sensor and the flow channel (Wu and Sansen, 2002).

The sensor consists of two electrochemical cells integrated in the flow channel. The upstream cell functions as an oxygen producer and the downstream electrochemical cell functions as an amperometric oxygen sensor. At the upstream electrochemical cell, the chemical reaction occurred as follow:

$$2H_2O_2 \rightarrow 4H^+ + O_2 + 4e^-$$

On the application of an electrical pulse, water is dissociated at the working electrode and a pulse of oxygen is released. After that, the oxygen pulse is transported to the downstream of electrochemical cell by convection and diffusion. At the downstream of electrochemical cell, the chemical reaction occurred as follow:

$$O_2 + 4H^+ + 4e^- \rightarrow 2H_2O$$

The concentration of oxygen determines the current of the oxygen sensor. The backward implicit finite difference simulation is applied to solve the governing equation, $\frac{\partial c}{\partial t} = D(\frac{\partial^2 c}{\partial x^2} + \frac{\partial^2 c}{\partial y^2} + \frac{\partial^2 c}{\partial z^2}) - (v_x \frac{\partial c}{\partial x} + v_y \frac{\partial c}{\partial y} + v_z \frac{\partial c}{\partial z})$, where c is the concentration of oxygen, D is the diffusion coefficient, v_x, v_y, and v_z represent the solution velocity profile in the x-, y- and z-direction.

Based on Figure 1.23, an oxygen pulse is produced at the upstream oxygen producer and transported to the downstream by convection and diffusion. On the passing of the oxygen pulses, peaks are formed on the current curves of the oxygen sensor as shown in Figure 1.23(a). The breadth of the current peak depends on the flow rate. Hence, the slower the flow rate, the wider the current peak. By observing Figure 1.23(b), there is a good linearity between the reciprocal volume flow rates and the positions of curve maxima.

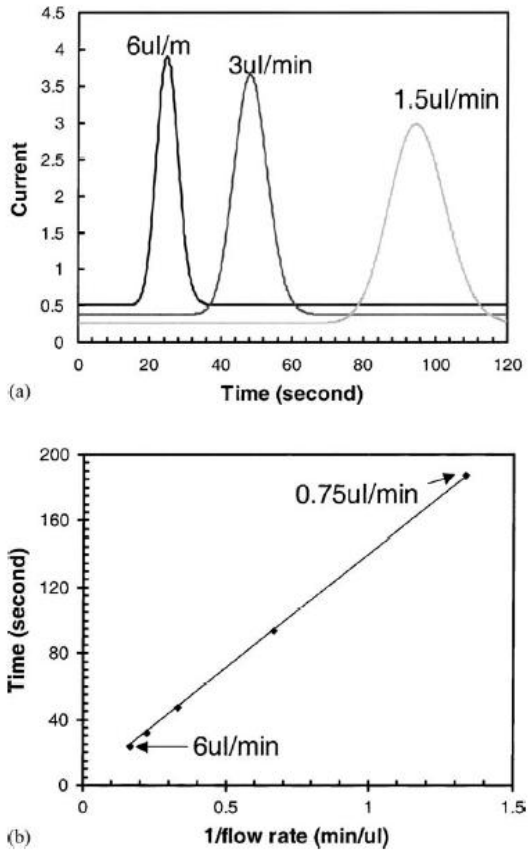

Figure 1.23: The simulation of the oxygen sensor at the different flow rates. (a) The current vs. time curves; (b) the relationship between the flow rate and the position of the current maximum (Wu and Sansen, 2002).

The experiment was also carried out and the corresponding results are shown in Figure 1.24. Arrow 'A' points at the application of the electrical pulse on the upstream cell, where the oxygen is produced. As already mentioned in the theoretical part above, the passing of the oxygen pulse on the working electrode, distinct peak forms on the current curve of the oxygen sensor. The experimental results also show that the oxygen pulse is deformed and broadened by convection and diffusion during the transportation. As the result, the positions of these peaks depend on the flow rates. The study concluded that both digital simulation and measurement results show the time difference between the production and detection of the oxygen pulse is only related to the flow rate. The detection range of the sensor is between 1 and 15µl/min.

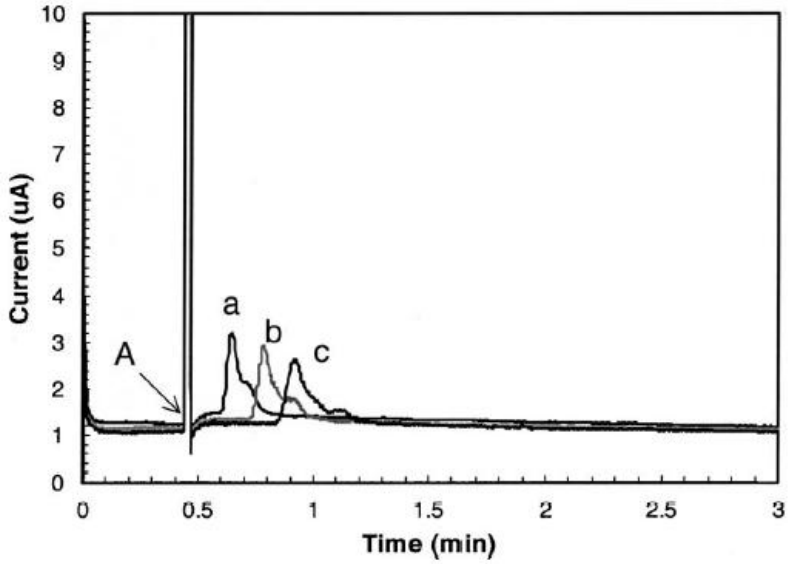

Figure 1.24: The current vs. time curves of the oxygen sensor at the different flow rates. Fluid: PBS. Flow rate: (a) 10µl/min; (b) 6µl/min; and (c) 4µl/min (Wu and Sansen, 2002).

Liu and Garimella (2003) have performed an investigation of liquid flow in micro channels. Figures 1.25 and 1.26 shows the apparatus that was used to conduct the experiment on the fluid flow in micro channel.

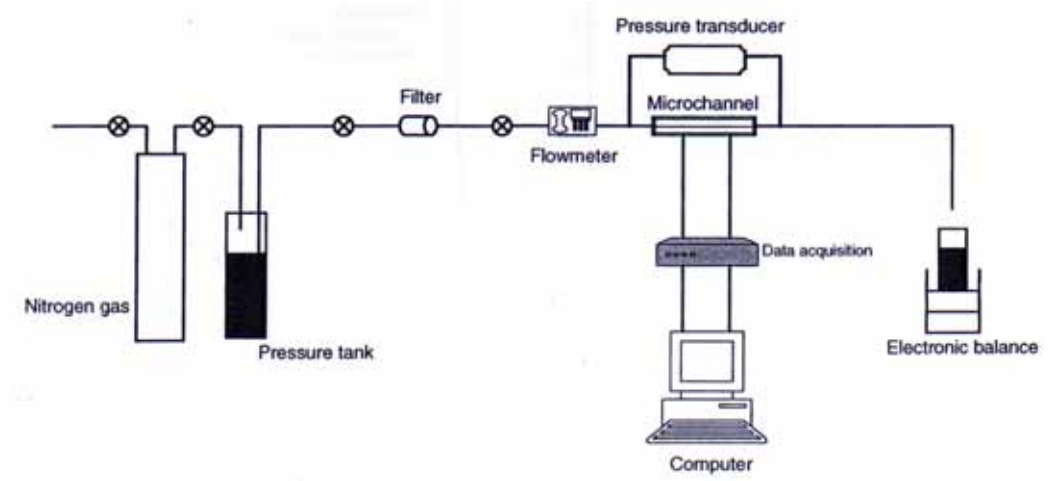

Figure 1.25: Schematic of the experimental apparatus (Liu and Garimella, 2003).

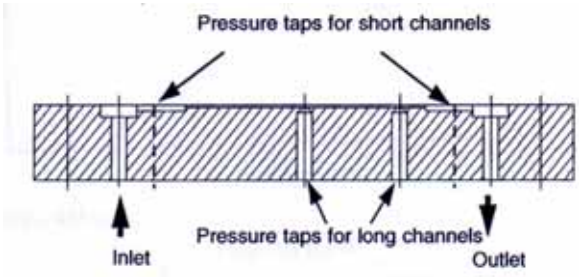

Figure 1.26: Schematic of the micro channel test section (Liu and Garimella, 2003).

After they conducted the experiment and analyzed the friction factor of the fluid flow in micro channel, they found that the experimental results agree closely with the theoretical predictions in the laminar region (see Figure 1.27). The experimental results also show that the friction factors deviate from the laminar region when the Reynolds number is approximately 2×10^3, which indicate the onset of transition. The

onset of transition of fluid flow for the micro channels are seen to agree with the behavior in conventional channels.

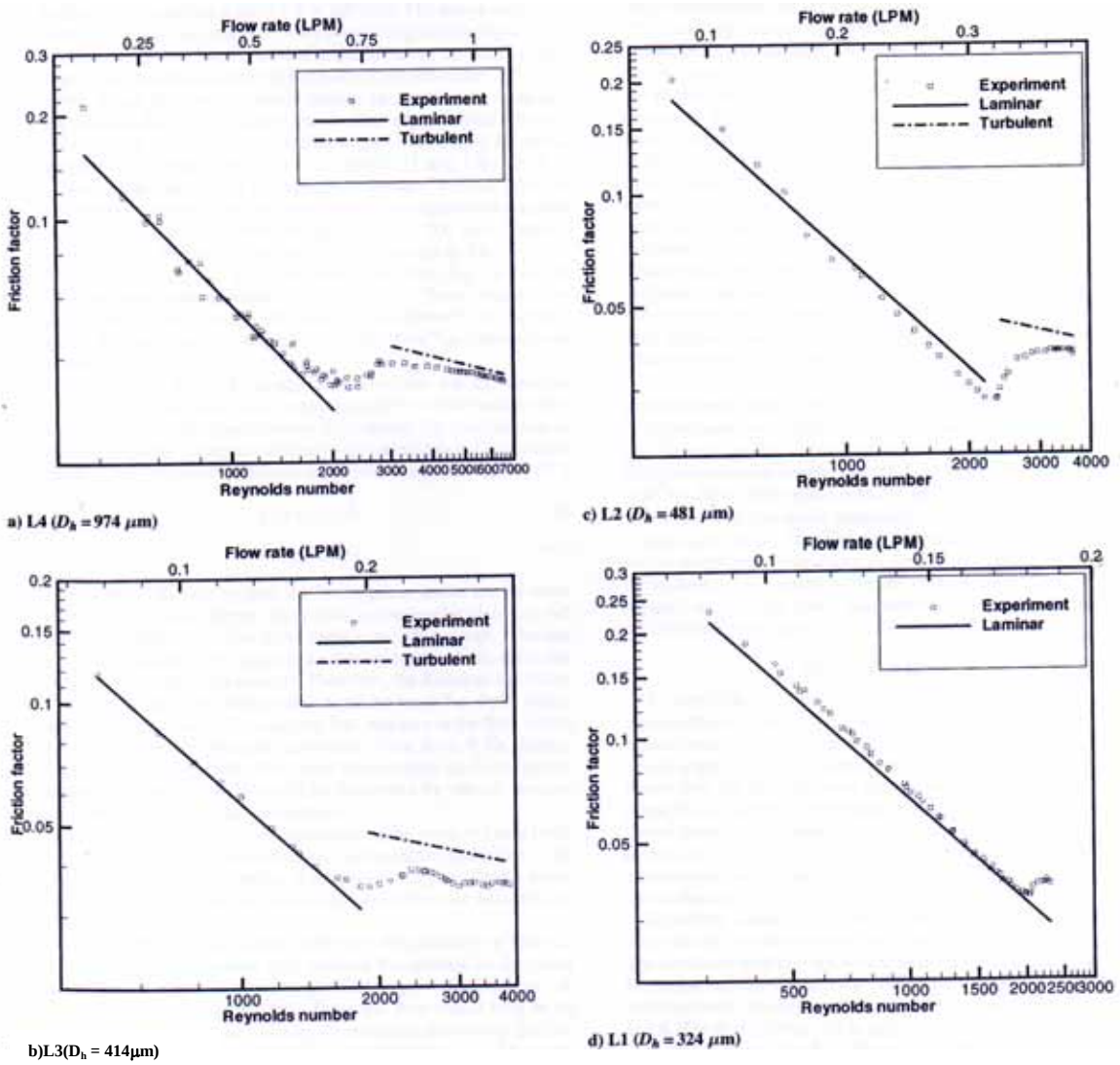

Figure 1.27: Friction factor variation with Reynolds number in 'long' micro channels (Liu and Garimella, 2003).

When they analyzed the onset of transition in micro channel, they found that the channel flow can stay laminar for Reynolds numbers of up to 50000 if completely undisturbed. With the presence of perturbations, the onset of turbulence will occur at $\mathrm{Re} = 1.8 \times 10^3$, below which the flow will remain laminar even with very strong

disturbances. Results from the present work also suggest that no such early transition occurs, at least down to hydraulic diameters of approximately 200μm. By observing Figure 1.27, especially in Figure 1.27(b) and Figure 1.27(c) indicate that the transition range extends up to Reynolds number of 4000. There are indications from Figure 1.27(a) that the flow becomes fully turbulent at $\mathrm{Re} = 5 \times 10^3$. These values compare favorably to $\mathrm{Re} = 3 \times 10^3$, which is considered to be the minimum Reynolds number for fully turbulent flow in conventional channels.

The examination on short micro channel had also been carried out in the experiment. The experimental results showed that good agreement between experiment and conventional correlations in the laminar regime, as shown in Figure 1.28.

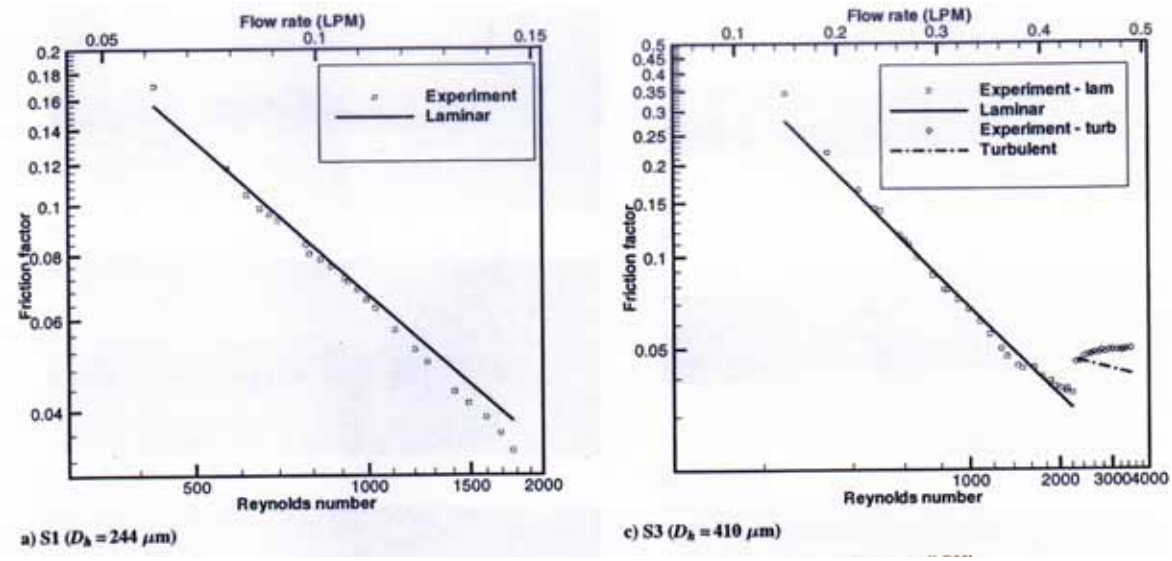

Figure 1.28: Corrected friction factor variation with Reynolds number in 'short' micro channels (Liu and Garimella, 2003).

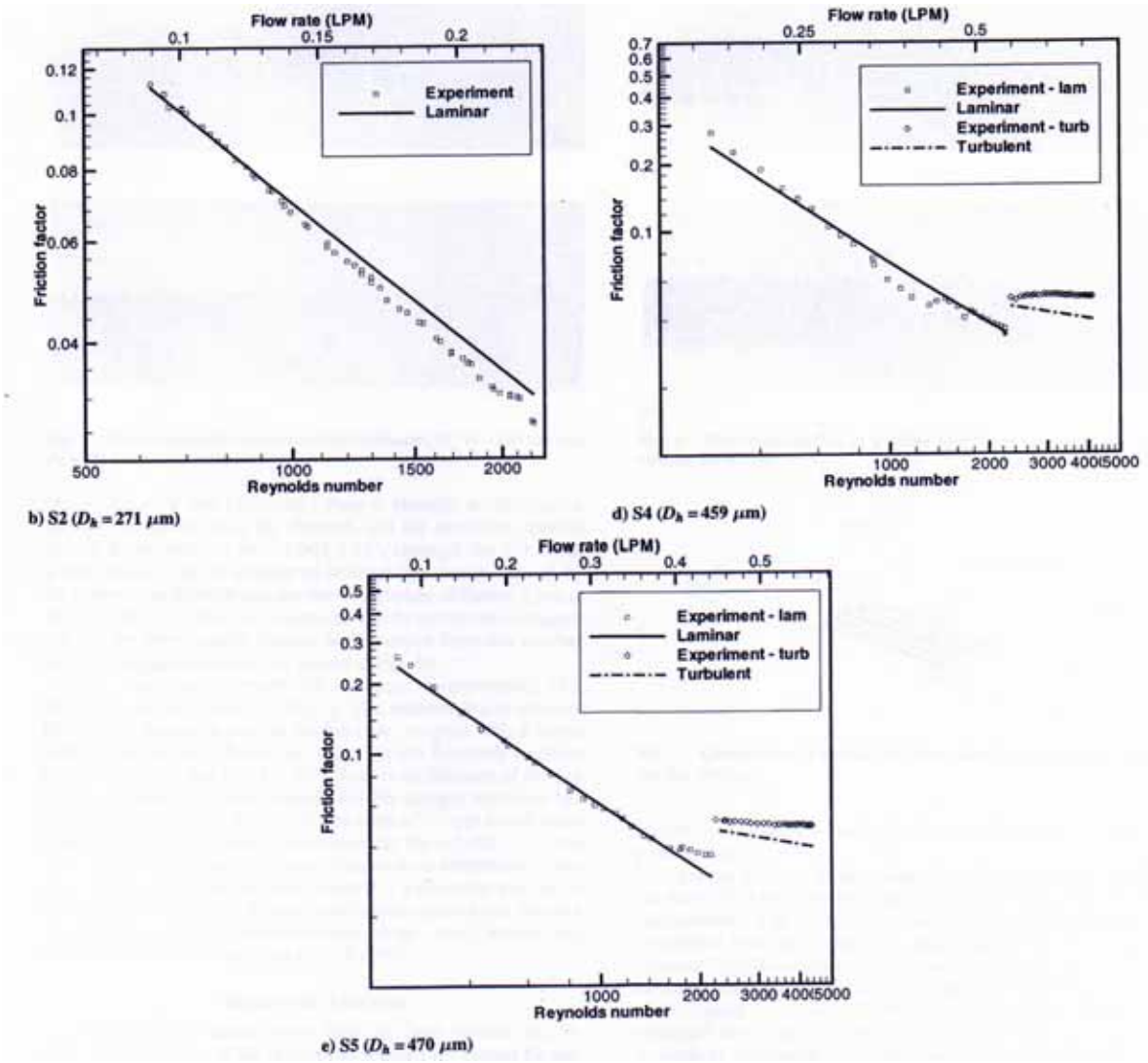

Figure 1.28: Corrected friction factor variation with Reynolds number in 'short' micro channels (cont') (Liu and Garimella, 2003).

Simulation by using a general – purposed finite volume – based computational fluid dynamics (CFD) software package (FLUENT) have been carried out. The calculation domain is shown in Figure 1.29. The results of the numerically predicted overall pressure drop in the micro channels against the experimentally measured overall pressure drop can be considered as satisfactory agreement, which are shown in Table 1.1.